Signatures of classical diffusion in quantum fluctuations of two-dimensional chaotic systems

Tsampikos Kottos, Alexander Ossipov, and Theo Geisel
Max-Planck-Institut für Strömungsforschung und Fakultät Physik der Universität Göttingen, Bunsenstraße 10, D-37073 Göttingen, Germany
(Received 8 July 2003; published 31 December 2003)

We consider a two-dimensional (2D) generalization of the standard kicked rotor and show that it is an excellent model for the study of universal features of 2D quantum systems with underlying diffusive classical dynamics. First we analyze the distribution of wave-function intensities and compare them with the predictions derived in the framework of diffusive *disordered* samples. Next, we turn the closed system into an open one by constructing a scattering matrix. The distribution of the resonance widths $\mathcal{P}(\Gamma)$ and Wigner delay times $\mathcal{P}(\tau_W)$ are investigated. The forms of these distributions are obtained for different symmetry classes and the traces of classical diffusive dynamics are identified. Our theoretical arguments are supported by extensive numerical calculations.

DOI: 10.1103/PhysRevE.68.066215 PACS number(s): 05.45.Mt, 73.23.−b

I. INTRODUCTION

Random matrix theory (RMT) was invented more than 50 years ago by Wigner in order to describe the statistical properties of complex nuclei [1]. In recent years the fast developments in mesoscopic physics and quantum chaos has given a new boost to the RMT approach [2,3]. The strength of RMT consists in the universality of its predictions containing no energy or length scales or any parameter dependence. At the same time this is its weakness, because it does not allow us to take into account various phenomena appearing in mesoscopic systems which introduce new length scales or parameters in the system.

The break down of *universality* and the traces of the underlying classical dynamics are important topics in quantum chaos studies and have major applications in mesoscopic physics. It is therefore highly important to compare the results from RMT models to the results from systems that have a semiclassical limit, and to look for circumstances where semiclassical tools rather than RMT become relevant. In this paper we extend our previous studies [4,5] on two-dimensional chaotic systems with underlying classical diffusion paying attention to applications of our results for random lasers and microwave absorption. We identify the signatures of classical diffusion in quantum fluctuations by analyzing the distribution of wave-function intensities of closed systems, and the resonance widths and Wigner delay times of their corresponding scattering analogs.

Our analysis is based on a two-dimensional (2D) generalization of the well-known kicked rotor (KR) model . For large values of the kicking strength the model is classically chaotic and the dynamics is diffusive. The detailed analysis of the classical system allows us to extract the relevant parameters that penetrate into the quantum-mechanical description. The quantum analog shows *dynamical* localization [6–9] with eigenstates which are exponentially localized in a similar fashion as the eigenstates of disordered systems. However here the localization occurs due to complicated interference effects created by the underlying classical chaotic dynamics. Attempts were made to put this analogy between the kicked rotor and disordered systems [7,10] on a solid base but the problem is still not solved completely [9].

Since the pioneering work of Anderson [11] it is known that the diffusion in *disordered* systems can be affected very strongly by quantum localization. If the system size exceeds the localization length, then the diffusion is completely suppressed after the time needed for the wave packet to spread over the scale of the localization length. But even in the absence of strong localization the existence of *prelocalized* states [12–20] influences the behavior of different physical quantities in the diffusive regime. Having this in mind, it is legitimate to ask, what happens with deterministic *chaotic* systems when quantum-mechanical description becomes relevant? Our analysis shows that prelocalized states are present also in the case of dynamical systems and affect various statistical quantities such as resonances and Wigner delay times. For the analysis of the latter quantities, we turned the closed KR to a scattering system by imposing ''absorption'' to a set of momentum states. The resulting scattering matrix is written in terms of the unitary evolution operator of the corresponding closed system and a projection operator. A detailed description of this construction is presented.

The paper is structured in the following way. In Sec. II the classical model is introduced and the main definitions are given. Sections III and IV are devoted to the corresponding quantum-mechanical system. The quantization on a torus is presented in Sec. III, while in Sec. IV we present a detailed construction of the scattering matrix. Sections V and VI are dedicated to the analysis of various statistical properties of the closed and the open 2D KR model correspondingly. Finally, our conclusions are summarized in Sec. VII.

II. THE CLASSICAL 2D KICKED ROTOR

A prominent example of a system with classical diffusion is, the well known in the field of quantum chaos, the KR model [6], which consists of the free propagating rotor driven periodically in time by an external force. Since the total energy of a driven system is not a constant of motion any more, the chaotic behavior can appear even in the 1D case.

Although many results are known for the standard 1D KR

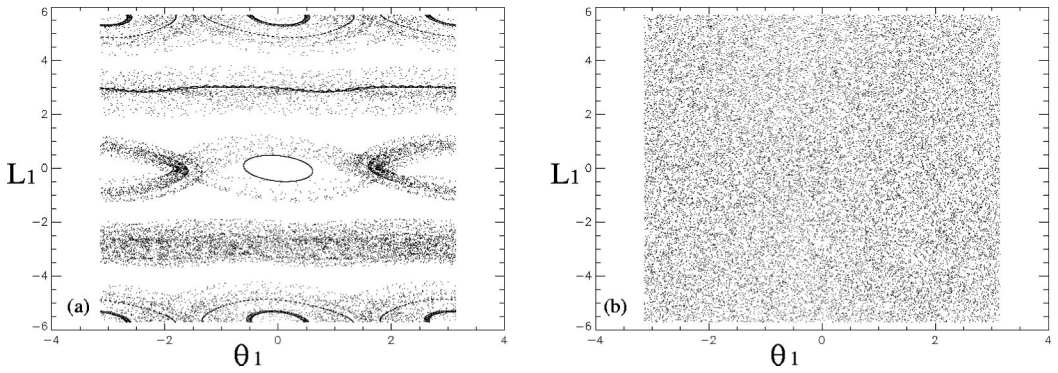

FIG. 1. Poincaré section of the classical phase space for Hamiltonian (1) for (a) $k=0.36$, (b) $k=6.37$.

there is almost no study for its two-dimensional generalization, besides Ref. [8] where the authors have focused on the analysis of dynamical evolution. The corresponding model is described by the following Hamiltonian:

$$H=H_0+kV(\{\theta_i\})\sum_m \delta(t-mT), \tag{1}$$

$$H_0(\{\mathcal{L}_i\})=\sum_{i=1}^{2}\frac{\tau_i}{2}(\mathcal{L}_i+\gamma_i)^2,$$

where the index $i=1$ (2) is related to the first (second) rotor correspondingly. $\mathcal{L}_i$ denotes the angular momentum and θ_i the conjugate angle of one rotor. The kick period is T, k is the kicking strength, while τ is a constant inversely proportional to the moment of inertia of the rotor. The parameter γ is an irrational number whose meaning will be explained below. The Hamiltonian (1) describes a system which is kicked periodically in time. Another representation of the Hamiltonian (1) may be given by one rotor moving on a two-dimensional sphere. The two rotors are interacting with each other by the potential

$$V(\{\theta_i\})=[\cos(\theta_1)\cos(\theta_2)\cos(\alpha) + \tfrac{1}{2}\sin(2\theta_1)\cos(2\theta_2)\sin(\alpha)]. \tag{2}$$

The parameter α breaks time-reversal symmetry (TRS). The form (2) was chosen so as to minimize the effect of symmetry breaking on the classical diffusion constant D (see below).

The classical equations of motion which correspond to the Hamiltonian (1) can be integrated over the kick period T giving a set of simple maps:

$$\theta_1(n+1)=\theta_1(n)+\tau_1 T\mathcal{L}_1(n) \mod 2\pi,$$

$$\theta_2(n+1)=\theta_2(n)+\tau_2 T\mathcal{L}_2(n) \mod 2\pi,$$

$$\mathcal{L}_1(n+1)=\mathcal{L}_1(n)-k\{-\sin[\theta_1(n+1)]\times\cos[\theta_2(n+1)]\cos(\alpha)+\cos[2\theta_1(n+1)]\times\cos[2\theta_2(n+1)]\sin(\alpha)\},$$

$$\mathcal{L}_2(n+1)=\mathcal{L}_2(n)-k\{-\cos[\theta_1(n+1)]\sin[\theta_2(n+1)]\times\cos(\alpha)-\sin[2\theta_1(n+1)]\times\sin[2\theta_2(n+1)]\sin(\alpha)\}, \tag{3}$$

where $\theta_i(n)$ and $\mathcal{L}_i(n)$ are the values of the dynamical variables taken just after the nth kick. The motion generated by this set of maps is integrable in the absence of the kicking potential. For sufficiently small but nonzero k the phase space of this system contains both regular islands and chaotic sea [see Fig. 1(a)]. When k is large enough then the dynamics becomes fully chaotic [see Fig. 1(b)] and there is diffusion in momentum space (Fig. 2) with diffusion coefficient

$$D\equiv\lim_{t\to\infty}\frac{\langle\mathcal{L}^2(t)\rangle}{t}\simeq\frac{k^2}{2T}. \tag{4}$$

The last expression is correct within the random-phase approximation [6,8,21] (see Appendix B).

The corresponding open system is described by the same set of equations (3) as the closed one, on top of which we add absorbing boundary conditions, namely, we set $\mathcal{L}_i$ equal to zero, if $\mathcal{L}_i<0$ or $\mathcal{L}_i>L$. These conditions give to "the particles" the possibility to escape from the system. The evolution of the classical density $\rho(x,y,t)$ is described by the Frobenius-Perron equation, which takes in our case the form of the following diffusion equation:

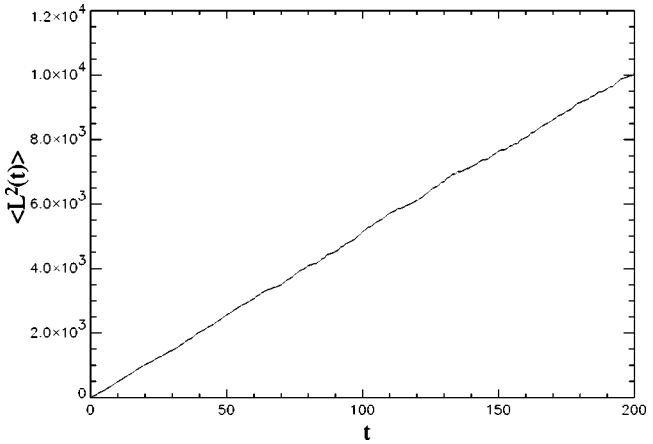

FIG. 2. Diffusion in momentum space for $k=9.1$.

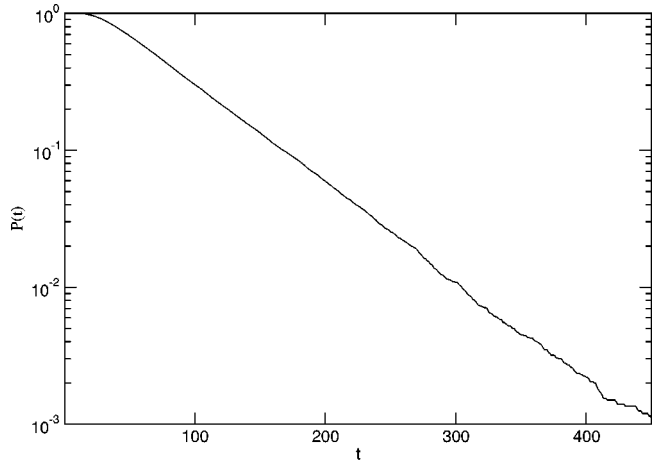

FIG. 3. Exponential decay of the classical survival probability for open kicked rotor model.

$$\frac{\partial \rho}{\partial t} = \frac{D}{4} \Delta \rho \tag{5}$$

with absorbing boundary condition

$$\vec{J}_n \equiv -\frac{D}{4} (\vec{\nabla} \rho)_n = -\Phi_n , \tag{6}$$

which sets the flux at the boundary $\vec{J}_n$ to be equal to the number of particles Φ_n carried out under one iteration of the map. The solution of Eqs. (5) and (6) can be represented as the superposition of the diffusive eigenmodes $v_k(x,y)$:

$$\rho(x,y,t) = \sum_{k=1}^{\infty} c_k e^{-\gamma_k t} v_k(x,y), \tag{7}$$

where γ_k are the corresponding eigenvalues and c_k are coefficients determined by the initial condition. The asymptotic behavior of the density is governed by the smallest eigenvalue $\gamma_1 \equiv \Gamma_{\rm cl}$. As a consequence one has an exponential decay of the classical survival probability $P(t) = \int\int dx dy\ \rho(x,y,t)$:

$$P(t) \propto e^{-\Gamma_{cl} t}. \tag{8}$$

The classical decay rate $\Gamma_{cl} \sim D/L^2$ can be estimated as the inverse time needed for the particle to reach the boundary (Thouless time). The exact value of the classical decay rate can be obtained as the solution of the corresponding eigenvalue problem or from the numerical calculation of $P(t)$. In Fig. 3 we present the results of our numerical calculations for $P(t)$ for some representative parameters.

III. QUANTIZATION ON A TORUS

Because of the periodicity of the external force a time-dependent solution of the KR model can be represented as a superposition of Floquet states [22]. These are the eigenstates of the evolution operator for one period (Floquet operator). For kicked systems the interaction with external force is instantaneous and one can factorize the total Floquet operator into the product of the evolution operators corresponding to the free propagation and the interaction. Due to this fact the kicked systems are very convenient for numerical study.

If the $\mathcal{L}_i$ are taken mod$(2\pi m_i / T\tau_i)$ where m_i are integers, Eq. (1) defines a dynamical system on a torus. The quantum mechanics of this system is described by a finite-dimensional time evolution operator for one period:

$$U = \exp[-iH_0(\{\mathcal{L}_i\})T/2] \exp[-iV(\{\theta_i\})] \times \exp[-iH_0(\{\mathcal{L}_i\})T/2], \tag{9}$$

where we put $\hbar = 1$. In the above representation, U is symmetric and describes the evolution in the middle of the rotations between two successive kicks. Upon quantization, additional symmetries associated with the discreteness of the momentum show up, which can be destroyed by introducing irrational values for the parameters γ_i's. The most striking consequence of quantization is the suppression of classical diffusion in momentum space due to quantum dynamical localization [6,7]. We introduce the eigenstate components $\mathbf{\Psi}_k(n)$ of the Floquet operator in the momentum representation by

$$\sum_m U_{mn} \mathbf{\Psi}_k(n) = e^{i\omega_k T} \mathbf{\Psi}_k(n). \tag{10}$$

The quantities ω_k are known as quasienergies, and their density is $\rho = T/2\pi$. The corresponding mean quasienergy spacing is $\Delta = 1/(\rho L^d)$, where L is the linear size of the system and d is the dimensionality ($d=2$ in our case). The Heisenberg time is $t_H = 2\pi/\Delta$ while $t_D = L^2/D$ is the diffusion time (Thouless time). Now one can formally define a dimensionless conductance as

$$g = t_H / t_D = D_k L^{d-2}, \tag{11}$$

where $D_k = TD$ is the diffusion coefficient measured in number of kicks. Four length scales are important here: the wavelength λ, the mean free path l_M, the linear extent of the system L, and the localization length ξ. In the rest of this paper we will always assume that

$$\lambda \ll l_M \ll L \ll \xi. \tag{12}$$

The first condition ensures that transport between scattering events may be treated semiclassically. This limit can be achieved for our system (1) when $k \to \infty$, $T \to 0$ while the classical parameter $K = kT$ remains constant. When $l_M \ll L$ as long as the motion is not localized (i.e., $L \ll \xi$) it is diffusive, since a particle scatters many times before it can traverse the system. The resulting mean free path for our system (1) is $l_M \simeq \sqrt{D_k}$ (see Appendix A) while the localization length for $d=1$ is $\xi \simeq D_k/2$ [6] and for $d=2$ is $\xi \simeq l_M e^{D_k/2}$ [8,23].

A great advantage of the kicked rotor consists in the fact that due to the unitarity of the evolution operator all its eigenstates have the same statistical properties. This is in contrast to the eigenstates of Hamiltonian models (such as Anderson model), where the eigenstates belonging to differ-

ent parts of the spectrum have different statistical properties and therefore they must be picked up from a narrow energy window. This allow us to collect a huge set of numerical data and perform a rather accurate numerical analysis. The results of our investigation will be discussed in Sec. V.

IV. THE SCATTERING APPROACH

To proceed with the analysis of the resonance widths and delay times we turn the closed 2D KR model (9) into an open one. To this end we impose ''absorption'' at the boundary of a square sample of size $L\times L$ in the momentum space in complete analogy with the classical setup. In other words, every time that one of the components of the two-dimensional momentum $(\mathcal{L}_1,\mathcal{L}_2)$ takes on the value 1 or L, the particle leaves the sample. The corresponding unitary scattering matrix S (see Appendix C) is given [24] by

$$S(\omega)=\sqrt{I-WW^{\dagger}}-WU\frac{1}{e^{-i\omega}-\sqrt{I-W^{\dagger}W}U}W^{\dagger}, \quad (13)$$

where I is the $L^2\times L^2$ unit matrix and W is an $M\times L^2$ matrix with matrix elements

$$W_{i,j}(k,A)=\begin{cases} w_i, & i=j \\ 0, & i\neq j \end{cases} \quad (14)$$

with $w_i^2\in[0,1]$ the tunnel probability in mode i. In the case of perfect coupling, which is considered here, $w_i=1$. Then $WW^{\dagger}=I_{M\times M}$ and $W^{\dagger}W$ is an $L^2\times L^2$ diagonal matrix with M nonzero elements equal to one. From the physical point of view, W describes at which ''site'' of the $L\times L$ sample we attach M ''leads'' [in our case $M=4(L-1)$]. Here $W^{\dagger}W$ is a projection operator onto the boundary, while $P\equiv I-W^{\dagger}W$ is the complementary projection operator which satisfies

$$\sqrt{I-W^{\dagger}W}=I-W^{\dagger}W. \quad (15)$$

Taking this into account, the expression (13) can be simplified:

$$S(\omega)=-WU\frac{1}{e^{-i\omega}-(I-W^{\dagger}W)U}W^{\dagger}$$

$$=WU\frac{1}{U-e^{-i\omega}-W^{\dagger}WU}W^{\dagger} \quad (16)$$

and using the unitarity of the evolution operator U we can rewrite the last expression as follows:

$$S=W\frac{1}{I-W^{\dagger}W-U^{\dagger}e^{-i\omega}}W^{\dagger}. \quad (17)$$

The scattering matrix (17) can equivalently be written in the form used conventionally in quantum chaotic scattering:

$$S(\omega)=-WUe^{i\omega}\frac{1}{I-e^{i\omega}PU}W^{\dagger}. \quad (18)$$

The scattering matrix S_{ij} given by Eq. (18) can be interpreted in the following way: once a wave enters the sample, it undergoes multiple scattering induced by $[I-e^{i\omega}PU]^{-1}=\sum_{n=0}^{\infty}(e^{i\omega}PU)^n$ until it is transmitted out. It is clear therefore that the matrix $\tilde{U}=PU$ propagates the wave inside the sample. However, contrary to the closed system in which the evolution operator is unitary, the absorption breaks the unitarity of the evolution matrix $\tilde{U}$.

The eigenvalues of $\tilde{U}$ occurring at complex quasienergies $\tilde{\omega}_n=\omega_n-(i/2)\Gamma_n$ are the poles of the scattering matrix. They represent long-lived intermediate states to which bound states of a closed system are converted due to coupling to continua. Here ω_n and Γ_n are the (dimensionless) position and width of the resonances, respectively.

Having at our disposal the scattering matrix S we can calculate the Wigner-Smith delay time. It captures the time-dependent aspects of quantum scattering and formally it is defined as

$$\tau_W(\omega)=-i\frac{d}{d\omega}\ln\det S(\omega) \quad (19)$$

and can be interpreted as the typical time an almost monochromatic wave packet remains in the interaction region.

A generalization of the notion of Wigner delay time is given through the Wigner-Smith operator. The latter is defined as (for the kicked rotor model one should use quasienergy instead of energy in the definition of Wigner-Smith operator)

$$Q=\frac{1}{i}S^{\dagger}\frac{\partial S}{\partial\omega}. \quad (20)$$

Introducing a new operator

$$K\equiv\frac{1}{I-W^{\dagger}W-U^{\dagger}e^{-i\omega}} \quad (21)$$

and taking the derivative of both sides of Eq. (17) we obtain

$$\frac{\partial S}{\partial\omega}=W\frac{\partial K}{\partial\omega}W^{\dagger}$$

$$=W\frac{1}{I-W^{\dagger}W-U^{\dagger}e^{-i\omega}}(-i)e^{-i\omega}U^{\dagger}$$

$$\times\frac{1}{I-W^{\dagger}W-U^{\dagger}e^{-i\omega}}W^{\dagger}$$

$$=-ie^{-i\omega}WKU^{\dagger}KW^{\dagger}. \quad (22)$$

Then the definition of the Wigner-Smith yields

$$Q=-ie^{-i\omega}WK^{\dagger}W^{\dagger}WKU^{\dagger}KW^{\dagger}. \quad (23)$$

The Wigner delay time can be expressed as the sum of proper delay times τ_q. The latter are the eigenvalues of the Wigner-Smith operator (23).

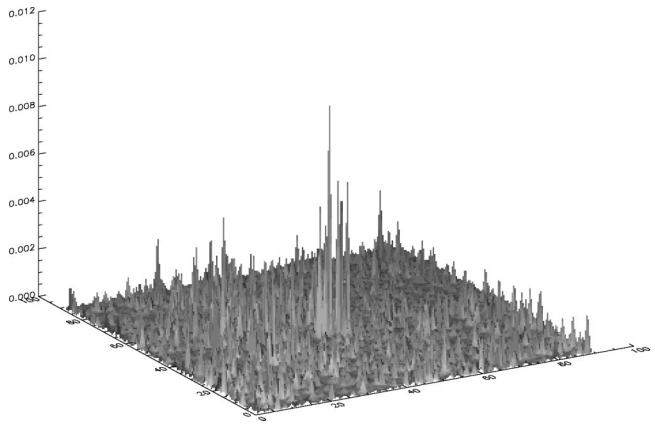

FIG. 4. An example of anomalously localized state. The size of the system is $L\times L=90\times 90$, the diffusion coefficient $D=33.8$.

V. DISTRIBUTION OF EIGENFUNCTION INTENSITIES

The statistical properties of wave-function intensities have sparked a great deal of research activity in recent years. These studies are not only relevant for mesoscopic physics [12–20,25–30], but also for understanding phenomena in areas of physics, ranging from nuclear [31] and atomic [32,33] to microwave physics [34–37] and optics [38]. Experimentally, using microwave cavity techniques it is possible to probe the microscopic structure of electromagnetic wave amplitudes in chaotic or disordered cavities [34–37]. Recently, the interest in this problem was renewed when new effective-field theoretical techniques were developed for the study of the distribution of eigenfunction intensities $\mathcal{P}(|\psi|^2)$ of *random* Hamiltonians. As the disorder increases, these results predict that the eigenfunctions become increasingly nonuniform, leading to an enhanced probability of finding anomalously large eigenfunction intensities in comparison with the random matrix theory prediction. Thus, the notion of *prelocalized* states, i.e., states which are localized much more strongly than typical eigenstates, has been introduced [12–17] to explain the appearance of long tails in the distributions of the conductance and other physical observables [12].

Up to now all theoretical predictions [12–20,25,30] and numerical calculations [27–29] apply to disordered systems and are based on an ensemble averaging over disorder realizations. Their validity, however, for a quantum *dynamical* system (with a well-defined classical limit) that behaves diffusively is not evident. Here we show that prelocalized states exist also for dynamical systems with underlying classical diffusion and investigate the effect of these states in $\mathcal{P}(|\psi|^2)$. An example of them is reported in Fig. 4. Our main conclusion is that in a generic dynamical system with classical diffusion, $\mathcal{P}(|\psi|^2)$ is described quite well by the nonlinear σ model (NLSM). We point out that between the various theoretical works there is a considerable disagreement about the parameters that control the shape of $\mathcal{P}(|\psi|^2)$ and their dependence on TRS. More specifically, the NLSM suggests that the tail of $\mathcal{P}(|\psi|^2)$ in two dimensions is sensitive to TRS [16–19,25], while a direct optimal fluctuation (DOF) method predicts a symmetry independent result [20]. This prediction was an additional motivation for the present study.

In the following section we calculate the distribution function $\mathcal{P}(y=L^d|\Psi_k(n)|^2)$ by using a direct diagonalization of the Floquet operator (9). The TRS is broken entirely for $\alpha=5.749$, i.e., the phase difference for a typical trajectory and its time-reversal counterpart is larger than 2π, so that all interference effects between time-reversal trajectories are suppressed. In order to test the issue of dynamical correlations, we randomize the phases of the kinetic term of the evolution operator (9) and calculate the resulting $\mathcal{P}(y)$. This model will be referred to as random-phase KR (RPKR). Since all our eigenfunctions have the same statistical properties (in contrast to the Anderson cases where one should pick up only eigenfunctions having eigenenergies within a small energy interval [27–29]) we make use of all of them in our statistical analysis. The classical parameter $K>6.36$ is large enough in all cases to exclude the existence of any stability islands in phase space, the accelerator modes known for KR [21,39] are avoided as well. The influence of the accelerator modes on the eigenfunction statistics is an interesting problem, which is out of the scope of the present study and deserves a separate investigation. The classical diffusion coefficient D_k is calculated numerically by iterating the classical map obtained from Eq. (1). Below we present our numerical results and compare them to the predictions of Refs. [13–20,25].

A. Numerical results

Let us start our numerical analysis from the ballistic regime where $g\to\infty$. In this case, RMT is applicable and one finds [3]

$$\mathcal{P}^{RMT}_{(\beta=1)}(y)=\exp(-y/2)/\sqrt{2\pi y}, \tag{24}$$

$$\mathcal{P}^{RMT}_{(\beta=2)}(y)=\exp(-y). \tag{25}$$

Here β denotes the corresponding Dyson ensemble: $\beta=1(2)$ for preserved (broken) TRS. This result can be easily understood. Indeed, within the random matrix theory one assumes that all the eigenvector components are independent (the normalization of the eigenvector is not essential in the thermodynamic limit, i.e., when the number of its components becomes very large) random variables obeying Gaussian distribution. Going to the distribution of the modulus square of the components one immediately recovers Eq. (24). For the case of the broken time-reversal symmetry one should take into account that each component has statistically independent real and imaginary parts, leading to the distribution given by Eq. (25). The numerical data presented in Fig. 5 show that the distributions of the eigenfunction intensities in the ballistic regime for the two-dimensional kicked rotor are described very nicely by the RMT prediction.

As the ratio between the system size and the localization length increases, the deviations from the RMT results of the body and the tails of the distribution $\mathcal{P}_\beta(y)$ become noticeable and can be parametrized by a single parameter which is the dimensionless conductance $g=D_k$. For $y<D_k$, according to all studies [14–18] $\mathcal{P}(y)$ is just the RMT result with

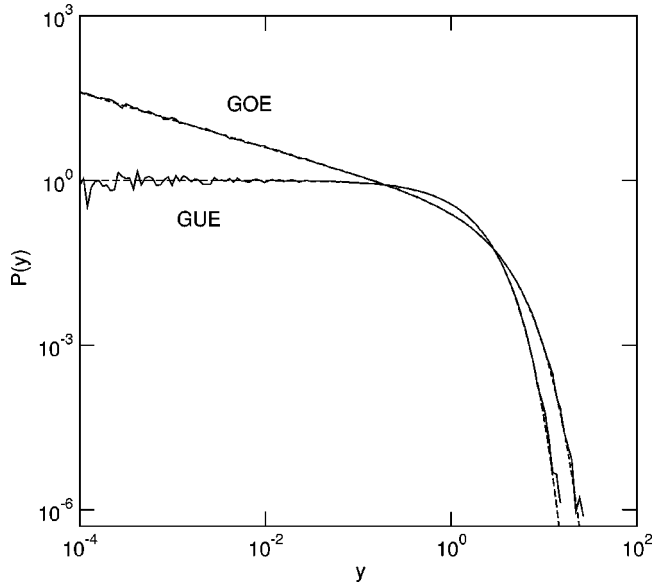

FIG. 5. Distributions of the eigenfunction intensities in the ballistic regime for two-dimensional kicked rotor (solid lines) compared with the RMT predictions (dashed lines).

polynomial corrections in powers of L/D_k, i.e., $\mathcal{P}_\beta(y) = \mathcal{P}_\beta^{RMT}(y)[1+\delta\mathcal{P}_\beta(y)]$. The leading term of this expansion is given by

$$\delta\mathcal{P}_\beta(y) \simeq \kappa \begin{cases} 3/4 - 3y/2 + y^2/4 & \text{for } \beta=1 \\ 1 - 2y + y^2/2 & \text{for } \beta=2, \end{cases} \tag{26}$$

where κ is the 2D diffusion propagator (time-integrated return probability), which is identical for $\beta=1$ and $\beta=2$ since it is a classical quantity.

Figures 6(a) and 6(b) show corrections to $\mathcal{P}_\beta^{RMT}$ for $g = D_k \gg 1$ for two representative values of D_k. We find again that the form of the deviations are very well described by Eq. (26) and the agreement becomes better for larger values of the diffusion constant. This is due to the fact that by increasing D_k we are approaching the semiclassical region and therefore Eqs. (12) are better satisfied. At the same time higher-order corrections in $\delta\mathcal{P}_\beta(y)$ become negligible with respect to the leading term given by Eq. (26).

In Fig. 6(c) we summarize our results for various D_k values. The extracted κ_β values are obtained by the best fit of the data to Eq. (26). Again we find that κ_β depends linearly on $1/D_k$. However, κ_1 and κ_2 are different. Moreover the best fit with $\kappa_\beta = A_\beta D_k^{-1} + B_\beta$ yields $A_{\beta=1} = 5.44 \pm 0.03$ and $A_{\beta=2} = 10.84 \pm 0.04$ indicating that the ratio $R = A_2/A_1$ is close to 2, a value that could be explained on the basis of ballistic effects [19,25,27,29]. Taking the latter into account leads to an additional term in the classical propagator $\kappa_\beta = \kappa_{diff} + (\beta/2)\kappa_{ball}$. The first term is the one discussed previously and is associated with long trajectories which are of diffusive nature while the latter one is associated with short ballistic trajectories which are self-tracing [19,25]. Thus, when $\kappa_{diff} \ll \kappa_{ball}$ we get $R=2$. The calculation with the RPKR model shows, however, that the corresponding ratio is $R \simeq 1$ in agreement with the theoretical prediction for disordered systems with a pure diffusion. This indicates that dynamical correlations can be important.

For the tails of the distributions, the result of the NLSM within a saddle-point approximation [16,17,19,25] is

$$\mathcal{P}_\beta(y) \simeq \exp[-C_\beta^\sigma (\ln y)^2], \quad C_\beta^\sigma = \frac{\beta\pi^2\rho}{2}\frac{D}{\ln(L/l)}. \tag{27}$$

Note that the decay in the tails of Eq. (27) depends on β. Recently, a DOF method was used to calculate the tails of $\mathcal{P}_\beta(y)$ [20] for the white-noise random potential. It was

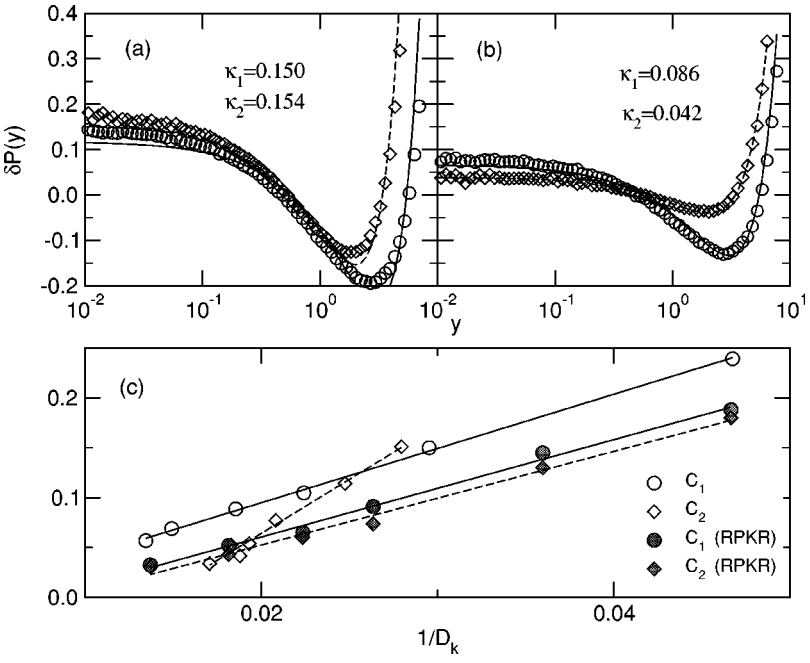

FIG. 6. Corrections to the distribution intensities $\delta\mathcal{P}_\beta(y)$ for the two-dimensional kicked rotator model (9). The system size is $L=90$, ($\bigcirc$) $\beta=1$, ($\diamond$) $\beta=2$. The solid (dashed) lines are the best fit of Eq. (26) for $\beta=1(2)$ to the numerical data: (a) $D_k \approx 34$ and (b) $D_k \approx 53$; (c) fit parameters κ_β vs D_k^{-1}. The solid (dashed) lines are the best fits to $\kappa_\beta = A_\beta D_k^{-1} + B_\beta$ for $\beta=1(2)$.

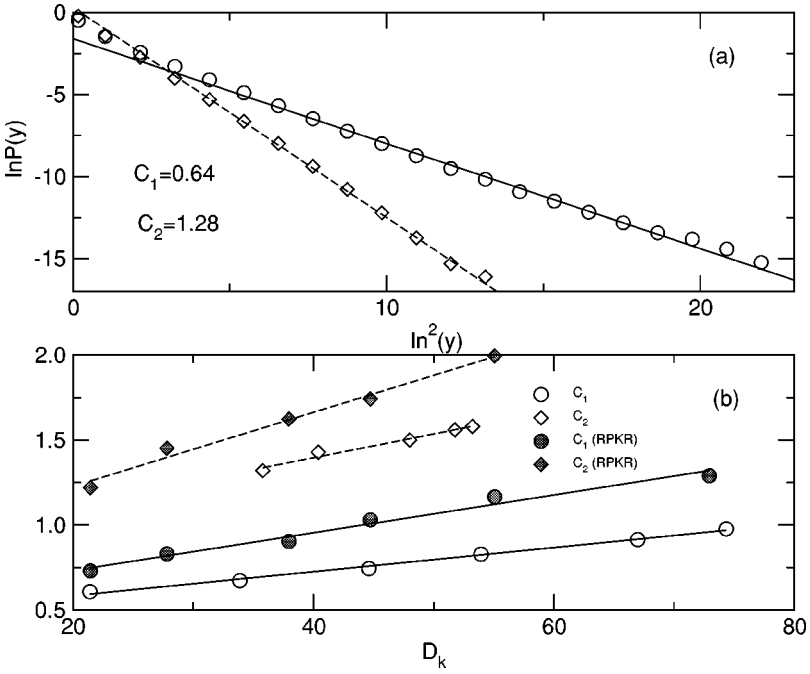

FIG. 7. (a) Tails of the distribution $\mathcal{P}_{\beta=1}(y>D_k)$ for the model (9) and $D_k \simeq 35$. The system size is $L=80$, (○) $\beta=1$, (◇) $\beta=2$. The solid (dashed) lines are the best fit of Eq. (27) for $\beta=1(2)$ to the numerical data. (b) Fitted log-normal coefficients C_β vs the classical diffusion coefficient D_k. The solid (dashed) lines are the best fits to $C_\beta = A_\beta D_k + B_\beta$ for $\beta=1(2)$.

found that the tails are still given by Eq. (27) but with a log-normal coefficient C which is independent of the parameter β:

$$C^{\mathrm{DOF}} = \pi^2 \rho \frac{D}{\ln(L/\lambda)}. \tag{28}$$

Figure 7(a) shows a representative case of $\mathcal{P}_{\beta=1}(y>D_k)$. The tails show a log-normal behavior predicted by Eq. (27). In Fig. 7(b) we report the log-normal coefficients C_β extracted from the best fit to our numerical data versus the classical diffusion coefficient. A pronounced linear behavior is observed in agreement with both theories. However one clearly sees that C_1 differs from C_2 in contrast to the DOF prediction (28) and to recent numerical calculations done for the 2D Anderson model [27]. We point out here that in Ref. [27] the authors were not able to go to large enough values of conductance g (in comparison to our study) where the theory can really be tested. In contrast, the NLSM predicts a value of 2 for the ratio $R=C_2^\sigma/C_1^\sigma$. We note that C_β^σ is only the leading term in D_k. In order to calculate this ratio, we performed a fit to our data with $C_\beta = A_\beta D_k + B_\beta$. The resulting ratio was found to be $R=A_2/A_1=1.97\pm0.03$ in perfect agreement with the NLSM predictions. Finally in Fig. 7(b) we also present our results for the RPKR model [using the same data as the one in Fig. 6(c)]. Again we found that the ratio $R=1.96\pm0.03\approx 2$. Thus $\mathcal{P}(y>D_k)$ depends on TRS and is described by the NLSM. The fact that the prediction of a DOF method is not observed in our calculations might be due to nonuniversal (depending on the type of disorder) character of this result.

VI. OPEN SYSTEMS: DISTRIBUTION OF RESONANCES AND DELAY TIMES

In this section we analyze the statistical properties of resonances $\mathcal{P}(\Gamma)$ and Wigner delay times $\mathcal{P}(\tau)$ for a 2D diffusive system. This study is important for various applications among which are diffusive random lasers and microwave cavities [40–44] where most of the theoretical treatment is limited by RMT. We point out here that current developments of microwave experiments in random dielectric media in the diffusive regime [45] may allow us a direct comparison between theory and experiment.

Specifically, we have found that the resonance width distribution $\mathcal{P}(\Gamma)$ is given by

$$\mathcal{P}(\Gamma<\Gamma_{cl}) \sim \exp[-C_\beta(\ln\Gamma)^2], \quad \text{where } C_\beta \sim \beta D,$$

$$\mathcal{P}(\Gamma \gtrsim \Gamma_{cl}) \sim \sqrt{\frac{D}{L^2}} \frac{1}{\Gamma^{3/2}} \tag{29}$$

while the distribution of the Wigner delay times is given by the following expressions:

$$\mathcal{P}(\tau \lesssim \Gamma_{cl}^{-1}) \sim \frac{1}{\tau^{3/2}} \exp(-\sigma/\tau),$$

$$\mathcal{P}(\tau > \Gamma_{cl}^{-1}) \sim \exp[-C_\beta(\ln\tau)^2], \tag{30}$$

where D is the classical diffusion constant, β denotes the symmetry class, and σ is some constant of order unity.

Our theoretical considerations are supported by numerical calculations for the open analog of the 2D KR model described in Secs. II and IV. The parameters of the model were chosen in such a way that the conditions (12) discussed in the preceding section were fulfilled. In order to improve our statistics, we randomized the phases of the kinetic term of the evolution operator (9) and used a number of different realizations. The results of the preceding section allow us to conclude that this procedure does not change the universal features of the model. In all cases we had at least 60 000 data for statistical processing.

A. Resonance widths distribution

For diffusive mesoscopic samples, there is no systematic investigation of $\mathcal{P}(\Gamma)$ besides Ref. [46] where the authors have focused on the large tails of $\mathcal{P}(\Gamma)$ for a quasi-1D system in the diffusive regime. This deficiency is felt especially strong in the random-laser community where one wants to know the statistical properties of the lasing threshold.

Usually we model random laser as a disordered or chaotic system containing a dye that is able to amplify the radiation with a rate η, in a certain frequency interval. In contrast to the traditional lasers where the necessary feedback is due to mirrors at the boundaries of the laser cavity, the key mechanism for random lasers is the multiple-scattering inside the medium [40]. The lasing threshold is given by the value of the smallest decay rate (i.e., smallest resonance width) of all eigenmodes in the amplification window [47,48]. The underlying reasoning is that in the mode with the smallest decay rate the photons are created faster by amplification than they can leave (decay) the sample.

Assuming that the number of modes $K \gg 1$ that lie in the frequency window where the amplification is possible have resonance widths Γ that are statistically independent one gets for distribution of lasing thresholds $\tilde{\mathcal{P}}(\Gamma)$ [47–49]:

$$\tilde{\mathcal{P}}(\Gamma) = K\mathcal{P}(\Gamma \ll 1)\left[1 - \int_0^{\Gamma} \mathcal{P}(\Gamma' \ll 1)\, d\Gamma'\right]^{K-1}, \quad (31)$$

where we have assumed that all K resonances are distributed according to $\mathcal{P}(\Gamma \ll 1)$. The validity of this approximation was verified recently in the framework of the RMT [50]. An important outcome of our study will be that one can identify traces of prelocalized states in the latter distribution and consequently in $\tilde{\mathcal{P}}(\Gamma)$. This sheds some light on recent experimental finding for random lasers which suggests the appearance of localized modes in diffusive samples [51].

We start our analysis with the study of resonance width distribution $\mathcal{P}(\Gamma)$ for $\Gamma < \Gamma_{cl}$. The small resonances $\Gamma < \Delta$ can be associated with the existence of prelocalized states of the closed system which were discussed in the preceding section. They consist of a short-scale bump (where most of the norm is concentrated) and they decay rapidly in a power-law fashion from the center of localization [20,25]. One then expects that states of this type with localization centers at the bulk of the sample are affected very weakly by the opening of the system at the boundaries. In first-order perturbation theory, considering the opening as a small perturbation we obtain

$$\frac{\Gamma}{2} = \langle \Psi | W^{\dagger} W | \Psi \rangle = \sum_{n \in \text{boundary}} |\Psi(n)|^2 \sim L |\Psi(L)|^2, \quad (32)$$

where $|\Psi(L)|^2$ is the wave-function intensity of a prelocalized state at the boundary. At the same time the distribution of $\theta = 1/\sqrt{L}\Psi(L)$ for large values of the argument is found to be of log-normal type [20]:

$$\mathcal{P}(\theta) \sim \exp[-\pi^2 D \ln^2(\theta^2)]. \quad (33)$$

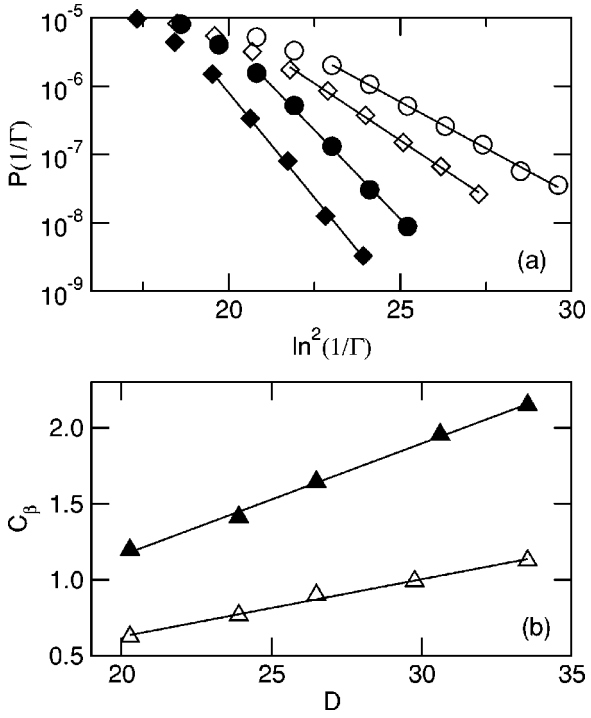

FIG. 8. (a) The distribution of resonance widths [plotted as $\mathcal{P}(1/\Gamma)$ vs $1/\Gamma$] for $\Gamma < \Gamma_{cl}$ for two representative values of D. The system size in all cases is $L = 80$. Filled symbols correspond to broken TRS. The solid lines are the best fit of Eq. (29) for $\beta = 1(2)$ to the numerical data. (b) Coefficients C_β vs D. The solid lines are the best fits to $C_\beta = A_\beta D + B_\beta$ for $\beta = 1(2)$. The ratio $R = A_2/A_1 = 1.95 \pm 0.03$

Using this together with Eq. (32) we obtain

$$\mathcal{P}(1/\Gamma) \sim \exp[-\pi^2 D \ln^2(1/\Gamma)]. \quad (34)$$

We would like to stress that, based on the results of the preceding section, the expression for $\mathcal{P}(\theta)$ must be corrected by including the TRS factor β in the exponent. Taking all the above into account we end up with the expression given in Eq. (29).

The numerical data reported in Fig. 8 support the validity of the above considerations. However, we would like to mention that the perturbative argument is valid only for the case of very small resonances, i.e., $\Gamma < \Delta$, whereas our numerical data indicate that one can extend the log-normal behavior of $\mathcal{P}(\Gamma)$ up to resonances with $\Delta < \Gamma < \Gamma_{cl}$.

Next we turn to the analysis of $\mathcal{P}(\Gamma)$ for $\Gamma \gtrsim \Gamma_{cl}$. In Fig. 9(a) we report our numerical results for $\mathcal{P}(\Gamma)$ with preserved (broken) TRS for two representative values of D. An inverse power law $\mathcal{P}(\Gamma) \sim \Gamma^{-1.5}$ is evident in accordance with Eq. (29). [The behavior of the extreme large Γ tails of $\mathcal{P}(\Gamma)$ is essentially determined by the coupling to the leads which is model dependent. Their relative number is proportional to $M/L^2 \sim L^{-1}$ and therefore they are statistically insignificant.] From the figure it is clear that this part of the distribution is independent of the symmetry class, in contrast to the small resonance distribution discussed above.

The following argument provides some understanding of the behavior of $\mathcal{P}(\Gamma)$ for $\Gamma \gtrsim \Gamma_{cl}$. First we need to recall that

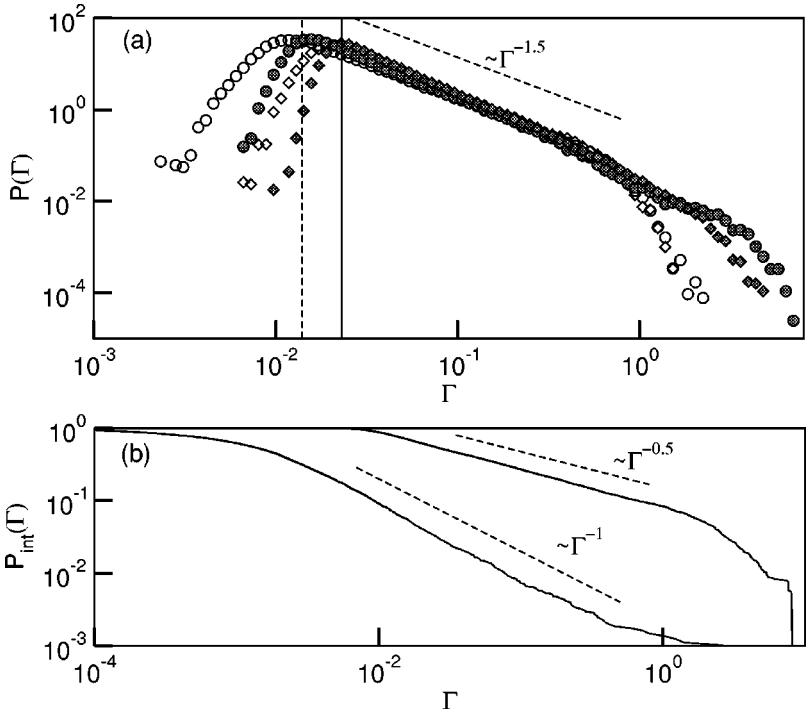

FIG. 9. (a) The resonance width distribution $\mathcal{P}(\Gamma)$ for preserved TRS and $D=20.3$ ($\bigcirc$) and $D=33.5$ ($\diamond$). The corresponding filled symbols represent $\mathcal{P}(\Gamma)$ for broken TRS and the same values of D. The dashed (solid) vertical line marks the classical decay rate Γ_{cl} for $D=20.3$ ($D=33.5$). (b) The $\mathcal{P}_{\rm int}(\Gamma)$ for a sample with nine leads (lower curve). For comparison we plot also the $\mathcal{P}_{\rm int}(\Gamma)$ for the same sample but when we open the system from the boundaries. The dashed lines correspond to the theoretical predictions (36) and (37).

the inverse of Γ represents the quantum lifetime of a particle in the corresponding resonant state escaping into the leads. Moreover we assume that the particles are uniformly distributed inside the sample and diffuse until they reach the boundaries, where they are absorbed. Then we can associate the corresponding lifetimes with the time $t_R\sim 1/\Gamma_R\sim R^2/D$ a particle needs to reach the boundaries, when starting a distance R away. This classical picture can be justified for all states with $\Gamma\gtrsim\Gamma_{cl}\sim D/L^2$. The relative number of states that require a time $t<t_R$ in order to reach the boundaries (or equivalently the number of states with $\Gamma>\Gamma_R$) is

$$\mathcal{P}_{\rm int}(\Gamma_R)=\int_{\Gamma_R}^{\infty}\mathcal{P}(\Gamma)d\Gamma\sim\frac{S(t_R)}{L^2}, \tag{35}$$

where $S(t_R)$ is the area populated by all particles with lifetimes $t<t_R$. In the case of open boundaries we get

$$\mathcal{P}_{\rm int}(\Gamma_R)\sim\frac{L^2-(L-2R)^2}{L^2}\sim\sqrt{\frac{\Gamma_{cl}}{\Gamma_R}}-\frac{\Gamma_{cl}}{\Gamma_R}. \tag{36}$$

For $\Gamma_R>\Gamma_{cl}$ the first term in the above equation is the dominant one and thus Eq. (29) follows.

Here it is interesting to point out that a different way of opening the system might lead to a different power-law behavior for $\mathcal{P}(\Gamma)$. Such a situation can be realized if instead of opening the system at the boundaries we introduce ''one-site'' absorber (or one ''lead'') somewhere in the sample. In such a case we have

$$\mathcal{P}_{\rm int}(\Gamma_R)\sim\frac{S(t_R)}{L^2}=\frac{R^2}{L^2}=\frac{Dt_R}{L^2}\sim\frac{\Gamma_{cl}}{\Gamma_R}. \tag{37}$$

The above result is valid for any number M of ''leads'' such that the ratio M/L^2 scales as $1/L^2$. In Fig. 9(b) we report the integrated resonance width distribution $\mathcal{P}_{\rm int}(\Gamma)$ for the case with nine ''leads'' attached somewhere to the $2D$ sample.

A straightforward generalization of our arguments for 3D systems in the diffusive regime gives

$$\mathcal{P}_{\rm int}(\Gamma_R)\sim\sqrt{\frac{\Gamma_{cl}}{\Gamma_R}}-2\frac{\Gamma_{cl}}{\Gamma_R}+\frac{4}{3}\left(\frac{\Gamma_{cl}}{\Gamma_R}\right)^{3/2}, \tag{38}$$

which for $\Gamma_R>\Gamma_{cl}$ leads to the same universal expression as in Eq. (29). Similarly, the analog of Eq. (37) in 3D is

$$\mathcal{P}_{\rm int}(\Gamma_R)\sim\left(\frac{\Gamma_{cl}}{\Gamma_R}\right)^{3/2}. \tag{39}$$

It is interesting to compare the above prediction (29) with the results of the random matrix theory. In the general case, Fyodorov and Sommers [52] proved that the distribution of scaled resonance widths $\gamma=\Gamma/\Delta$ for the unitary random matrix ensemble is given by

$$\mathcal{P}(\gamma)=\frac{(-1)^M}{\Gamma(M)}\gamma^{M-1}\frac{d^M}{d\gamma^M}\left(e^{-\gamma\pi q}\frac{\sinh(\gamma\pi)}{(\gamma\pi)}\right), \tag{40}$$

where M is the number of open channels and the parameter q controls the degree of coupling with the channels ($q=1$ for perfect coupling). Our numerical data from the 2D KR model in the ballistic regime, reported in Fig. 10, are in excellent agreement with the theoretical prediction (40).

In the limit of $M\gg 1$, which is relevant for the comparison with Eq. (29), Eq. (40) reduces to the following expression [52]:

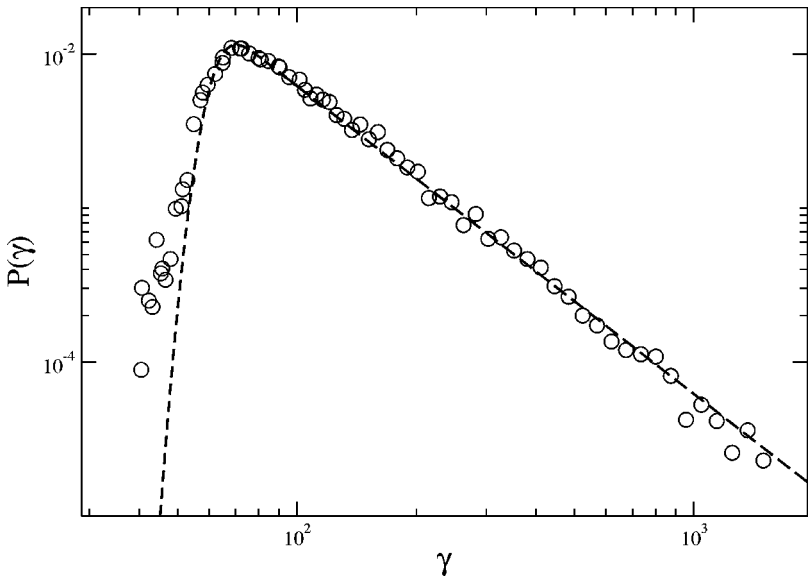

FIG. 10. Distributions of the resonance widths in the ballistic regime for two-dimensional kicked rotor (○) compared with the RMT predictions (dashed lines).

$$\mathcal{P}(\gamma)=\begin{cases}\dfrac{M}{2\pi\gamma^2} & \text{for } \dfrac{M}{\pi(q+1)}<\gamma<\dfrac{M}{\pi(q-1)}\\ 0 & \text{otherwise.}\end{cases} \quad (41)$$

One can see two essential distinctions between this result and Eq. (29). First, the power law $P(\Gamma)\sim 1/\Gamma^2$ is not the same as the power law predicted by Eq. (29) for large resonances $P(\Gamma)\sim 1/\Gamma^{3/2}$. Since this difference appears in the "classical" part of the distribution, it can be explained as a difference in the classical dynamics of a particle inside the system: ballistic (RMT) versus diffusive motion. Indeed, taking into account that for ballistic system $R\sim vt$ and $\Gamma_{cl}\sim v/L$, where v is the velocity of the particle, one immediately finds from Eq. (36) that $\mathcal{P}_{\rm int}(\Gamma_R)\sim\Gamma_{cl}/\Gamma_R$ for $\Gamma_R>\Gamma_{cl}$, in agreement with the RMT prediction $P(\Gamma)\sim 1/\Gamma^2$. Second, according to Eq. (41) there is a gap in the distribution of the resonance widths: there are no resonances with widths smaller than $M/\pi(g+1)$. The existence of the gap can be understood, if one relates the small resonances to the coupling of the wave functions to the leads. Since the wave functions in the RMT are extended, the probability to find a wave function, which is weakly coupled to all M channels, goes to zero when the number of channels becomes very large $M\gg 1$. In the diffusive regime, in contrast, there are prelocalized states, which are weakly coupled to the leads. Due to their existence the distribution of the small resonance widths has a nontrivial behavior described by Eq. (29).

B. Wigner delay times distribution

We turn now to the analysis of Wigner delay times and calculate their probability distribution. It can be shown that this distribution is related to the distribution of reflection coefficients R in the present of weak absorption. Absorption is one of the main ingredients in actual experimental situations and its theoretical understanding is of great importance. Unfortunately a comprehensive treatment of absorption is still lacking. There are only very few reported analytical results for the distribution of the reflection coefficient $\mathcal{P}(R)$ in the presence of absorption and all of them are either within the regime of applicability of RMT [41–44,53] or applied for quasi-1D geometry [53,54]. Here we will derive $\mathcal{P}(R)$ in the diffusive regime in two dimensions and in the weak absorption limit. In this limit it was shown [42,44] that the following relation between the proper Wigner delay times and reflection coefficients holds:

$$R_q=1-\tau_q/\tau_a, \quad (42)$$

where τ_q are the proper delay times (eigenvalues of the Wigner-Smith operator) and $1/\tau_a$ is the absorption rate. Thus the knowledge of $\mathcal{P}(R)$ reduces to the calculation of the distribution of proper Wigner delay times $\mathcal{P}(\tau_q)$ [42].

Below we make the standard assumption that the resulting distribution generated over different energies is equivalent with the one generated over different disorder realizations. Our starting point is the well-known relation

$$\tau(\omega)=\sum_{n=1}^{L^2}\frac{\Gamma_n}{(\omega-\omega_n)^2+\Gamma_n^2/4}, \quad (43)$$

which connects the Wigner delay times and the poles of the S matrix.

Let us start with the far tails. It is evident that large times $\tau(\omega)\sim\Gamma_n^{-1}$ corresponds to the cases when $\omega\simeq\omega_n$ and $\Gamma_n\ll 1$. In the neighborhood of these points, $\tau(\omega)$ can be approximated by a single Lorentzian (43). Sampling the quasienergies ω with step $\Delta\omega\ll\Gamma_{min}$ we calculate the number of points for which the time delay is larger than some fixed value τ (see Fig. 11). Assuming that the contribution of each Lorentzian is proportional to its width one can estimate this number as $\Sigma_{\Gamma_n<1/\tau}\Gamma_n/\Delta E$. For the integrated distribution of delay times in the limit $\Delta\omega\to 0$ we obtain

$$\mathcal{P}_{int}(\tau)\sim\int^{1/\tau}d\Gamma\mathcal{P}(\Gamma)\Gamma \quad (44)$$

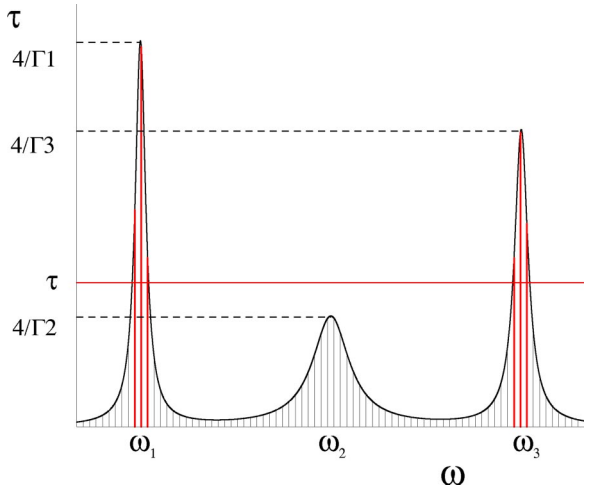

FIG. 11. Schematic plot for the Wigner delay time as a function of quasienergy according to Eq. (43).

and by substituting the small resonance width asymptotic given by Eq. (29) we come out with the log-normal law of Eq. (30) in agreement with our numerical findings reported in Fig. 12.

Now we estimate the behavior of $\mathcal{P}(\tau)$ for $\tau \lesssim \Gamma_{cl}^{-1}$. In this regime many short-living resonances contribute to the sum (43). We may therefore consider τ as a sum of many independent positive random variables each of the type $\tau_n = \Gamma_n x_n$, where $x_n = \delta\omega_n^{-2}$. Assuming further that $\delta\omega_n$ are uniformly distributed random numbers we find that the distribution $\mathcal{P}(x_n)$ has the asymptotic power-law behavior $1/x_n^{3/2}$. As a next step we find that the distribution $\mathcal{P}(\tau_n)$ decays asymptotically as $1/\tau_n^{3/2}$ where we use that $\mathcal{P}(\Gamma_n) \sim 1/\Gamma_n^{3/2}$. Then the corresponding $\mathcal{P}(\tau)$ is known to be a stable asymmetric Levy distribution $L_{\mu,1}(\tau)$ of index $\mu = 1/2$ [55] which has the form given in Eq. (30) at the origin. We point out here that the asymptotic behavior $\mathcal{P}(\tau) \sim 1/\tau^{3/2}$ emerges also for chaotic/ballistic systems where the assumption of uniformly distributed $\delta\omega_n$ is the only crucial ingredient (see, for example, Ref. [52]).

Since $\tau = \Sigma_{i=1}^{M} \tau_q$, we expect the behavior of the distribution of proper delay times $\mathcal{P}(\tau_q)$ to be similar to $\mathcal{P}(\tau)$ for large values of the arguments (for $\tau \gg 1$ we have $\tau \sim \tau_q^{\max}$). Moreover, from the numerical point of view $\mathcal{P}(\tau_q)$ can be studied in a better way because a larger set of data can be generated easily. Our numerical findings for $\mathcal{P}(\tau_q)$ are reported in Fig. 12 and are in nice agreement with Eq. (30), even for moderate values of τ_q. We stress here that the dashed lines in Fig. 12 have slopes equal to C_β taken from the corresponding log-normal tails of $\mathcal{P}(\Gamma)$.

Finally we would like to compare our result (30) with the results known from the random matrix theory. Although the distributions of the proper delay times [56,57] and partial delay times (defined as a derivative of the partial phase θ_i of the S matrix with respect to energy) [52] have been calculated recently, there is no explicit analytical formula for the distribution of the Wigner delay times for number of open channels $M > 2$ [58]. Nevertheless using consideration similar to one presented above (see the discussion for $\tau \lesssim \Gamma_{cl}^{-1}$) one can argue [52] that the part of $\mathcal{P}(\tau)$ for $\tau \lesssim \Gamma_{cl}^{-1}$ is the same in the RMT as stated in Eq. (30). However, the distribution of the large delay times in the RMT is expected to have a power-law behavior $\mathcal{P}(\tau) \sim 1/\tau^{2+\beta M/2}$ with M being the number of open channels. This is in contrast with a log-normal tail stated in Eq. (30).

VII. CONCLUSIONS

This paper is devoted to the investigation of chaotic and disordered systems characterized by the classical diffusion. Section V deals with study of the closed system. Specifically, we perform a detailed numerical analysis of the eigenfunction intensities $\mathcal{P}(y)$ of the two-dimensional kicked rotor on a torus. Our results indicated that the distribution $\mathcal{P}(y)$ of generic quantum *dynamical* systems with diffusive classical limit is affected by the existence of *prelocalized* states. The deviations from RMT are well described by field theoretical

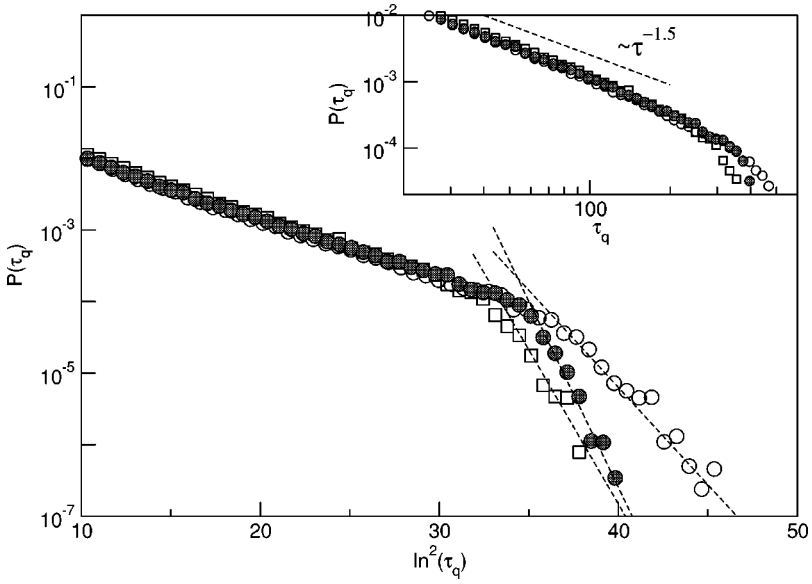

FIG. 12. The proper delay times distribution $\mathcal{P}(\tau_q)$ for $D = 20.3$ (○) and $D = 29.8$ (□). The (●) correspond to $D = 20.3$ but now with broken TRS. The dashed lines have slopes equal to C_β extracted from the corresponding $\mathcal{P}(\Gamma)$ (see Fig. 8). In the inset we report $\mathcal{P}(\tau_q)$ for moderate values of τ_q in a double logarithmic scale.

methods developed for disordered systems. In particular, we find that the dependence of the tails of $\mathcal{P}_\beta(y)$ on TRS is described correctly by NLSM.

Section VI deals with the study of the open system. After introducing a scattering formalism for the KR model we investigated the distribution of the resonance widths $\mathcal{P}(\Gamma)$ and Wigner delay times $\mathcal{P}(\tau)$. We obtain the forms of these distributions (log normal for large τ and small Γ, and power law in the opposite case) for different symmetry classes and show that they are determined by the underlying diffusive classical dynamics and by the existence of the prelocalized states. Our theoretical arguments are supported by extensive numerical calculations.

Although the arguments, we used to explain the behavior of $\mathcal{P}(\Gamma)$ and $\mathcal{P}(\tau)$, can be easily generalized to the three-dimensional case, the numerical test of these predictions has not been still performed. Moreover the study of three-dimensional case would allow us to investigate these distribution at the critical point of the metal-insulator transition. The first attempt to attack this problem was done in Ref. [59], but a detailed understanding is still required.

ACKNOWLEDGMENTS

We thank I. E. Smolyarenko for useful comments. This work was supported by a grant from the German-Israeli Foundation for Scientific Research and Development.

APPENDIX A: THE MEAN FREE PATH

Let us consider the evolution operator of the two-dimensional kicked rotor introduced in Eq. (9) (to simplify the calculations we put $T=1$)

$$U=e^{-iH_0(\mathcal{L}_1,\mathcal{L}_2)/2}e^{-iV(\theta_1,\theta_2)}e^{-iH_0(\mathcal{L}_1,\mathcal{L}_2)/2}. \tag{A1}$$

The set of the orthogonal eigenfunctions of the free Hamiltonian H_0 is given by plane waves in the angle representation

$$\phi_{(n_1,n_2)}(\theta_1,\theta_2)=\frac{1}{2\pi}e^{i(n_1\theta_1+n_2\theta_2)}. \tag{A2}$$

They are normalized in such a way that

$$\int_0^{2\pi}\int_0^{2\pi}d\theta_1 d\theta_2|\phi_{(n_1,n_2)}(\theta_1,\theta_2)|^2=1. \tag{A3}$$

Let us denote by $U_{(k_1,k_2),(n_1,n_2)}$ the matrix elements of the evolution operator in this basis

$$U_{(k_1,k_2),(n_1,n_2)}=\langle\phi_{(k_1,k_2)}|U|\phi_{(n_1,n_2)}\rangle. \tag{A4}$$

According to the definition of the evolution operator the modulus square of its elements have the meaning of the probability to change the initial momentum (n_1,n_2) to the final momentum (k_1,k_2) in one kick. Therefore one can define the *mean free path in momentum space* [8] by

$$l_M^2=\sum_{r_1}\sum_{r_2}(r_1^2+r_2^2)|U_{(0,0),(r_1,r_2)}|^2. \tag{A5}$$

Here we used the fact that $|U_{(k_1+m_1,k_2+m_2),(n_1+m_1,n_2+m_2)}|^2=|U_{(k_1,k_2),(n_1,n_2)}|^2$, so without loss of generality one can take the initial momentum equal to $(0,0)$. In order to calculate the right-hand side of Eq. (A5) we first give an explicit expression to the matrix elements $U_{(k_1,k_2),(n_1,n_2)}$:

$$\begin{aligned}U_{(k_1,k_2),(n_1,n_2)}&=\sum_{i,j,s,t}\langle\phi_{(k_1,k_2)}|e^{-iH_0(\mathcal{L}_1,\mathcal{L}_2)/2}|\phi_{(i,j)}\rangle\langle\phi_{(i,j)}|e^{-iV(\theta_1,\theta_2)}|\phi_{(s,t)}\rangle\langle\phi_{(s,t)}|e^{-iH_0(\mathcal{L}_1,\mathcal{L}_2)/2}|\phi_{(n_1,n_2)}\rangle\\&=e^{-i[H_0(k_1,k_2)+H_0(n_1,n_2)]/2}\langle\phi_{(k_1,k_2)}|e^{-iV(\theta_1,\theta_2)}|\phi_{(n_1,n_2)}\rangle e^{-i[H_0(k_1,k_2)+H_0(n_1,n_2)]/2}\frac{1}{4\pi^2}\\&\times\int_0^{2\pi}\int_0^{2\pi}d\theta_1 d\theta_2 e^{-iV(\theta_1,\theta_2)}e^{i(n_1-k_1)\theta_1+i(n_2-k_2)\theta_2}.\end{aligned} \tag{A6}$$

Taking $(k_1,k_2)=(0,0)$ and $(n_1,n_2)=(r_1,r_2)$ we obtain

$$U_{(0,0),(r_1,r_2)}=e^{-i[H_0(0,0)+H_0(r_1,r_2)]/2}\frac{1}{4\pi^2}\int_0^{2\pi}\int_0^{2\pi}d\theta_1 d\theta_2 e^{-iV(\theta_1,\theta_2)}e^{ir_1\theta_1}e^{ir_2\theta_2}. \tag{A7}$$

The substitution of this expression into Eq. (A5) yields

$$l_M^2=\sum_{r_1}\sum_{r_2}(r_1^2+r_2^2)\frac{1}{(4\pi^2)^2}\int_0^{2\pi}\int_0^{2\pi}\int_0^{2\pi}\int_0^{2\pi}d\theta_1 d\theta_2 d\tilde{\theta}_1 d\tilde{\theta}_2 e^{-i(V(\theta_1,\theta_2)-V(\tilde{\theta}_1,\tilde{\theta}_2))}e^{ir_1(\theta_1-\tilde{\theta}_1)}e^{ir_2(\theta_2-\tilde{\theta}_2)}. \tag{A8}$$

Taking into account that

$$r_1^2 e^{ir_1(\theta_1-\widetilde{\theta 1}_1)}=\frac{\partial^2}{\partial\theta_1\partial\tilde{\theta}_1}e^{ir_1(\theta_1-\widetilde{\theta 1}_1)} \tag{A9}$$

and that the same is valid for r_2 the partial integration of the Eq. (A8) gives

$$l_M^2=\sum_{r_1}\sum_{r_2}\frac{1}{(4\pi^2)^2}\int_0^{2\pi}\int_0^{2\pi}\int_0^{2\pi}\int_0^{2\pi}d\theta_1 d\theta_2 d\tilde{\theta}_1 d\tilde{\theta}_2\left(\frac{\partial^2}{\partial\theta_1\partial\tilde{\theta}_1}+\frac{\partial^2}{\partial\theta_2\partial\tilde{\theta}_2}\right)e^{-i[V(\theta_1,\theta_2)-V(\tilde{\theta}_1,\tilde{\theta}_2)]}e^{ir_1(\theta_1-\tilde{\theta}_1)}e^{ir_2(\theta_2-\tilde{\theta}_2)}. \tag{A10}$$

The summation of the exponents over r_1 and r_2 yields two δ functions:

$$\begin{aligned}l_M^2&=\frac{1}{4\pi^2}\int_0^{2\pi}\int_0^{2\pi}\int_0^{2\pi}\int_0^{2\pi}d\theta_1 d\theta_2 d\tilde{\theta}_1 d\tilde{\theta}_2\left(\frac{\partial^2}{\partial\theta_1\partial\tilde{\theta}_1}+\frac{\partial^2}{\partial\theta_2\partial\tilde{\theta}_2}\right)e^{-i[V(\theta_1,\theta_2)-V(\tilde{\theta}_1,\tilde{\theta}_2)]}\delta(\theta_1-\tilde{\theta}_1)\delta(\theta_2-\tilde{\theta}_2)\\&=\frac{1}{4\pi^2}\int_0^{2\pi}\int_0^{2\pi}\int_0^{2\pi}\int_0^{2\pi}d\theta_1 d\theta_2 d\tilde{\theta}_1 d\tilde{\theta}_2\left(\frac{\partial V}{\partial\theta_1}(\theta_1,\theta_2)\frac{\partial V}{\partial\tilde{\theta}_1}(\tilde{\theta}_1,\tilde{\theta}_2)+\frac{\partial V}{\partial\theta_2}(\theta_1,\theta_2)\frac{\partial V}{\partial\tilde{\theta}_2}(\tilde{\theta}_1,\tilde{\theta}_2)\right)\\&\quad\times e^{-i[V(\theta_1,\theta_2)-V(\tilde{\theta}_1,\tilde{\theta}_2)]}\delta(\theta_1-\tilde{\theta}_1)\delta(\theta_2-\tilde{\theta}_2)\\&=\frac{1}{4\pi^2}\int_0^{2\pi}\int_0^{2\pi}d\theta_1 d\theta_2\left[\left(\frac{\partial V}{\partial\theta_1}(\theta_1,\theta_2)\right)^2+\left(\frac{\partial V}{\partial\theta_2}(\theta_1,\theta_2)\right)^2\right].\end{aligned} \tag{A11}$$

The last expression can be written in a compact form

$$l_M^2=\frac{1}{4\pi^2}\int_0^{2\pi}\int_0^{2\pi}d\theta_1 d\theta_2\|\vec{\nabla}V(\theta_1,\theta_2)\|^2. \tag{A12}$$

Now we calculate the mean free path in the case where the potential $V(\theta_1,\theta_2)$ is given by Eq. (2):

$$\begin{aligned}V(\theta_1,\theta_2)=k[&\cos(\theta_1)\cos(\theta_2)\cos(\alpha)\\&+\tfrac{1}{2}\sin(2\theta_1)\cos(2\theta_2)\sin(\alpha)].\end{aligned} \tag{A13}$$

Taking the derivative of this expression with respect to θ_1 and θ_2 one has

$$\begin{aligned}\left(\frac{\partial V}{\partial\theta_1}(\theta_1,\theta_2)\right)^2=k^2(&\sin^2\theta_1\cos^2\theta_2\cos^2\alpha+\cos^2 2\theta_1\\&\times\cos^2 2\theta_2\sin^2\alpha-2\sin\theta_1\cos 2\theta_1\cos\theta_2\\&\times\cos 2\theta_2\cos\alpha\sin\alpha),\end{aligned}$$

$$\begin{aligned}\left(\frac{\partial V}{\partial\theta_2}(\theta_1,\theta_2)\right)^2=k^2(&\cos^2\theta_1\sin^2\theta_2\cos^2\alpha\\&+\sin^2 2\theta_1\sin^2 2\theta_2\sin^2\alpha\\&+2\cos\theta_1\sin 2\theta_1\sin\theta_2\sin 2\theta_2\cos\alpha\sin\alpha).\end{aligned} \tag{A14}$$

The integration over θ_1 and θ_2 yields for the mean free path

$$\begin{aligned}l_M^2&=\frac{1}{4\pi^2}k^2(\pi^2\cos^2\alpha+\pi^2\sin^2\alpha+\pi^2\cos^2\alpha+\pi^2\sin^2\alpha)\\&=\frac{k^2}{2},\end{aligned} \tag{A15}$$

which is the same result as the one derived in Ref. [8] for different potential $V(\theta_1,\theta_2)$.

APPENDIX B: DIFFUSION COEFFICIENT IN THE RANDOM-PHASE APPROXIMATION

Here we give for completeness of the presentation the derivation of the diffusion coefficient for our model (1), (2) in the random-phase approximation. We start by writing the classical maps Eq. (3) for the general form of the potential $V(\theta_1,\theta_2)$:

$$\begin{aligned}\theta_1(n+1)&=\theta_1(n)+\tau_1 T\mathcal{L}_1(n)\mod 2\pi,\\\theta_2(n+1)&=\theta_2(n)+\tau_2 T\mathcal{L}_2(n)\mod 2\pi,\\\mathcal{L}_1(n+1)&=\mathcal{L}_1(n)-\frac{\partial V}{\partial\theta_1}[\theta_1(n+1),\theta_2(n+1)],\\\mathcal{L}_2(n+1)&=\mathcal{L}_2(n)-\frac{\partial V}{\partial\theta_2}[\theta_1(n+1),\theta_2(n+1)]\\&\quad-\sin[2\theta_1(n+1)]\sin[2\theta_2(n+1)]\sin(\alpha).\end{aligned} \tag{B1}$$

The diffusion coefficient in momentum space is defined as

$$D=\lim_{t\to\infty}\frac{\langle \mathcal{L}_1^2(t)+\mathcal{L}_2^2(t)\rangle}{t}. \tag{B2}$$

The average in this expression is taken over an ensemble of trajectories, with different initial conditions. Using the classical maps for $\mathcal{L}_1$ and $\mathcal{L}_2$ we obtain

$$\begin{aligned}D=\lim_{n\to\infty}\frac{1}{nT}\Bigg[&\sum_{i=1}^{n}\Bigg\langle\left(\frac{\partial V}{\partial\theta_1}[\theta_1(i),\theta_2(i)]\right)^2\\&+\left(\frac{\partial V}{\partial\theta_2}[\theta_1(i),\theta_2(i)]\right)^2\Bigg\rangle\\&+\sum_{i=1}^{n}\sum_{j=1,j\neq i}^{n}\Bigg\langle\frac{\partial V}{\partial\theta_1}[\theta_1(i),\theta_2(i)]\frac{\partial V}{\partial\theta_1}[\theta_1(j),\theta_2(j)]\\&+\frac{\partial V}{\partial\theta_2}[\theta_1(i),\theta_2(i)]\frac{\partial V}{\partial\theta_2}[\theta_1(j),\theta_2(j)]\Bigg\rangle\Bigg].\end{aligned} \tag{B3}$$

For the large values of the kicking strength k, in a good approximation one can consider the phases $\theta_1(i)$ and $\theta_2(i)$ as random variables which are uncorrelated for different i and distributed uniformly in the interval $[0,2\pi]$. Using this random-phase approximation it is easy to show that only the diagonal terms in Eq. (B3) give nonzero contribution in the limit $n\to\infty$. Taking into account that the distribution of the phases is uniform one can convert the sum for the diagonal terms into an integral. Finally we obtain

$$\begin{aligned}D=\frac{1}{4\pi^2T}\int_0^{2\pi}\int_0^{2\pi}d\theta_1 d\theta_2\Bigg[&\left(\frac{\partial V}{\partial\theta_1}(\theta_1,\theta_2)\right)^2\\&+\left(\frac{\partial V}{\partial\theta_2}(\theta_1,\theta_2)\right)^2\Bigg].\end{aligned} \tag{B4}$$

Then the formula for the diffusion coefficient measured in number of kicks $D_k=TD$ is given by

$$D_k=\frac{1}{4\pi^2}\int_0^{2\pi}\int_0^{2\pi}d\theta_1 d\theta_2\|\vec{\nabla}V(\theta_1,\theta_2)\|^2, \tag{B5}$$

which has exactly the same form as one appearing in Eq. (A12). Thus we obtain that in the random-phase approximation the following relation between the mean free path and the diffusion coefficient is valid:

$$D_k=l_M^2=\frac{k^2}{2}. \tag{B6}$$

Therefore changing the kicking strength we can easy tune the diffusion constant or Thouless conductance (for disordered systems). This allows us to investigate various regimes: ballistic, diffusive, and localized.

APPENDIX C: UNITARITY OF THE *S* MATRIX

Let us rewrite the expression for S matrix (16) in a more symmetric way. To this end we use a series expansion for inverse operator in Eq. (16):

$$\begin{aligned}&[U-e^{-i\omega}-W^\dagger WU]^{-1}\\&\quad=\left[(U-e^{-i\omega})\left(I-\frac{1}{U-e^{-i\omega}}W^\dagger WU\right)\right]^{-1}\\&\quad=\left[I-\frac{1}{U-e^{-i\omega}}W^\dagger WU\right]^{-1}\frac{1}{U-e^{-i\omega}}\\&\quad=\sum_{k\geqslant 0}\left(\frac{1}{U-e^{-i\omega}}W^\dagger WU\right)^k\frac{1}{U-e^{-i\omega}}.\end{aligned} \tag{C1}$$

Substituting this expansion in Eq. (16) we obtain

$$\begin{aligned}S&=\sum_{k\geqslant 0}WU\left(\frac{1}{U-e^{-i\omega}}W^\dagger WU\right)^k\frac{1}{U-e^{-i\omega}}W^\dagger\\&=\sum_{k\geqslant 0}\left(WU\frac{1}{U-e^{-i\omega}}W^\dagger\right)^{k+1}=\frac{WU\dfrac{1}{U-e^{-i\omega}}W^\dagger}{I-WU\dfrac{1}{U-e^{-i\omega}}W^\dagger}\\&=\frac{W\dfrac{U}{U-e^{-i\omega}}W\dagger}{W\left(I-\dfrac{U}{U-e^{-i\omega}}\right)W^\dagger}=-\frac{W\dfrac{U}{U-e^{-i\omega}}W^\dagger}{W\dfrac{e^{-i\omega}}{U-e^{-i\omega}}W^\dagger}.\end{aligned} \tag{C2}$$

Now using the unitarity of the evolution operator U we can calculate the Hermitian conjugate S matrix:

$$\begin{aligned}S^\dagger&=-\frac{W\dfrac{U^{-1}}{U^{-1}-e^{i\omega}}W^\dagger}{W\dfrac{e^{i\omega}}{U^{-1}-e^{i\omega}}W^\dagger}=-\frac{W\dfrac{e^{-i\omega}}{e^{-i\omega}-U}W^\dagger}{W\dfrac{U}{e^{-i\omega}-U}W^\dagger}\\&=-\frac{W\dfrac{e^{-i\omega}}{U-e^{-i\omega}}W^\dagger}{W\dfrac{U}{U-e^{-i\omega}}W^\dagger}=S^{-1}.\end{aligned} \tag{C3}$$

Thus the unitarity of the S matrix is proven.

[1] E. Wigner, Ann. Math. **62**, 548 (1955); **65**, 203 (1957).
[2] K.B. Efetov, *Supersymmetry in Disorder and Chaos* (Cambridge University Press, New York, 1997).
[3] H.-J. Stöckmann, *Quantum Chaos: An Introduction* (Cambridge University Press, Cambridge, 1999).
[4] A. Ossipov, T. Kottos, and T. Geisel, Phys. Rev. E **65**, 055209(R) (2002).
[5] A. Ossipov, T. Kottos, and T. Geisel, Europhys. Lett. **62**, 719 (2003).
[6] F.M. Izrailev, Phys. Rep. **196**, 299 (1990); G. Casati, B.V. Chirikov, J. Ford, and F.M. Izrailev, Lect. Notes Phys. **93**, 334 (1979).
[7] S. Fishman, D.R. Grempel, and R.E. Prange, Phys. Rev. Lett. **49**, 509 (1982).
[8] E. Doron and S. Fishman, Phys. Rev. Lett. **60**, 867 (1988).
[9] S. Jitomirskaya, Proc. ICM **3**, 445 (2003); J. Bourgain, Ann. Math. **156**, 249 (2002); J. Bourgain and S. Jitomirskaya, Invent. Math. **148**, 453 (2002).
[10] A. Altland and M.R. Zirnbauer, Phys. Rev. Lett. **77**, 4536 (1996).
[11] P.W. Anderson, Phys. Rev. **109**, 1492 (1958).
[12] B.L. Altshuler, V.E. Kravtsov, and I.V. Lerner, *Mesoscopic Phenomena in Solids* (North-Holland, Amsterdam, 1991), p. 449.
[13] B.A. Muzykantskii and D.E. Khmelnitskii, Phys. Rev. B **51**, 5480 (1995).
[14] Y.V. Fyodorov and A.D. Mirlin, Int. J. Mod. Phys. B **8**, 3795 (1994).
[15] Y.V. Fyodorov and A.D. Mirlin, Phys. Rev. B **51**, 13 403 (1995).
[16] V.I. Falko and K.B. Efetov, Europhys. Lett. **32**, 627 (1995).
[17] V.I. Falko and K.B. Efetov, Phys. Rev. B **52**, 17 413 (1995).
[18] A.D. Mirlin, J. Math. Phys. **38**, 1888 (1997).
[19] A.D. Mirlin, in *New Directions in Quantum Chaos*, Proceedings of the International School of Physics ''Enrico Fermi,'' Course CXLIII, edited by G. Casati, I. Guarneri, and U. Smilansky (IOS Press, Amsterdam, 2000).
[20] I.E. Smolyarenko and B.L. Altshuler, Phys. Rev. B **55**, 10 451 (1997).
[21] G.M. Zaslavsky, M. Edelman, and B.A. Niyazov, Chaos **7**, 159 (1997).
[22] L.E. Reichl, *The Transition to Chaos* (Springer-Verlag, New York, 1992).
[23] A. Lee and T.V. Ramakrishnan, Rev. Mod. Phys. **57**, 287 (1985).
[24] Y.V. Fyodorov and H.-J. Sommers, JETP Lett. **72**, 422 (2000).
[25] A.D. Mirlin, Phys. Rep. **326**, 259 (2000).
[26] U. Meirav, M.A. Kastner, and S.J. Wind, Phys. Rev. Lett. **65**, 771 (1990); U. Sivan *et al.*, Europhys. Lett. **25**, 605 (1994).
[27] V. Uski, B. Mehlig, R.A. Römer, and M. Schreiber, Phys. Rev. B **62**, R7699 (2000).
[28] B.K. Nikolić, Phys. Rev. B **64**, 014203 (2001).
[29] V. Uski, B. Mehlig, and M. Schreiber, Phys. Rev. B **63**, 241101(R) (2001).
[30] V.M. Apalkov, M.E. Raikh, and B. Shapiro, Phys. Rev. Lett. **89**, 126601 (2002).
[31] V. Zelevinsky, B.A. Brown, N. Frazier, and M. Horoi, Phys. Rep. **276**, 85 (1996).
[32] A.F. Brunello, T. Uzer, and D. Farrelly, Phys. Rev. Lett. **76**, 2874 (1996).
[33] G. Benenti, G. Casati, and D.L. Shepelyansky, Phys. Rev. A **56**, 3297 (1997).
[34] H.-J. Stöckmann and J. Stein, Phys. Rev. Lett. **64**, 2215 (1990).
[35] S. Sridhar, Phys. Rev. Lett. **67**, 785 (1991).
[36] A. Kudrolli, V. Kidambi, and S. Sridhar, Phys. Rev. Lett. **75**, 822 (1995).
[37] P. Pradhan and S. Sridhar, Phys. Rev. Lett. **85**, 2360 (2000).
[38] J.U. Nockel and A.D. Stone, Nature (London) **385**, 45 (1997); C. Gmachl *et al.*, Science **280**, 1556 (1998).
[39] A. Iomin and G.M. Zaslavsky, Chem. Phys. **284**, 3 (2002); G.M. Zaslavsky, Phys. Rep. **371**, 461 (2002).
[40] D.S. Wiersma, M.P. Van Albada, and A. Lagendijk, Nature (London) **373**, 203 (1995); D.S. Wiersma and A. Lagendijk, Phys. World **10**(1), 33 (1997).
[41] E. Kogan, P.A. Mello, and H. Liqun, Phys. Rev. E **61**, R17 (2000).
[42] C.W.J. Beenakker and P.W. Brouwer, Physica E (Amsterdam) **9**, 463 (2001).
[43] D.V. Savin and H.-J. Sommers, Phys. Rev. E **68**, 036211 (2003).
[44] E. Doron, U. Smilansky, and A. Frenkel, Phys. Rev. Lett. **65**, 3072 (1990).
[45] A.A. Chabanov, Z.Q. Zhang, and A.Z. Genack, Phys. Rev. Lett. **90**, 203903 (2003).
[46] F. Borgonovi, I. Guarneri, and D.L. Shepelyansky, Phys. Rev. A **43**, 4517 (1991).
[47] T.S. Misirpashaev and C.W.J. Beenakker, Phys. Rev. A **57**, 2041 (1998).
[48] M. Patra and C.W.J. Beenakker, Phys. Rev. A **60**, 4059 (1999); K.M. Frahm, H. Schomerus, M. Patra, and C.W.J. Beenakker, Europhys. Lett. **49**, 48 (2000); H. Schomerus, K.M. Frahm, M. Patra, and C.W.J. Beenakker, Physica A **278**, 469 (2000).
[49] M. Patra, Phys. Rev. E **67**, 016603 (2003); e-print cond-mat/0302506.
[50] Y.V. Fyodorov and B. Mehlig, Phys. Rev. E **66**, 045202 (2002); Y.V. Fyodorov and H.-J. Sommers, J. Phys. A **36**, 3303 (2003).
[51] H. Cao, Y. Ling, J.Y. Xu, and A.L. Burin, Phys. Rev. E **66**, 025601 (2002).
[52] Y.V. Fyodorov and H.-J. Sommers, J. Math. Phys. **38**, 1918 (1997).
[53] Y.V. Fyodorov, JETP Lett. **78**, 250 (2003).
[54] T.Sh. Misirpashaev and C.W.J. Beenakker, JETP Lett. **64**, 319 (1996).
[55] J.-P. Bouchaud and A. Georges, Phys. Rep. **195**, 127 (1990).
[56] P.W. Brouwer, K.M. Frahm, and C.W.J. Beenakker, Phys. Rev. Lett. **78**, 4737 (1997).
[57] H.-J. Sommers, D.V. Savin, and V.V. Sokolov, Phys. Rev. Lett. **87**, 094101 (2001).
[58] D.V. Savin, Y.V. Fyodorov, and H.-J. Sommers, Phys. Rev. E **63**, 035202(R) (2001).
[59] T. Kottos and M. Weiss, Phys. Rev. Lett. **89**, 056401 (2002).